Computer Modeling in Engineering & Sciences

Tech Science Press

https://doi.org/10.32604/cmes.2026.082594

ARTICLE

Efficient Structural Reliability Analysis via Adaptive Hidden Neuron Screening in Extreme Learning Machines

Yunlong Teng[1], **Ying Liu**[2], **Jianhong Liang**[1] **and Jinshang Luo**[3,*]

[1]School of Electronic Information and Electrical Engineering, Chengdu University, Chengdu, China
[2]School of Mechanical and Electrical Engineering, University of Electronic Science and Technology of China, Chengdu, China
[3]Information Center, University of Electronic Science and Technology of China, Chengdu, China

*Corresponding Author: Jinshang Luo. Email: jsluo@uestc.edu.cn

Received: 18 March 2026; Accepted: 02 May 2026; Published: 30 June 2026

ABSTRACT: Over the past decades, surrogate model-aided reliability analysis approaches grounded in active learning have undergone extensive development. However, Gaussian process models like Kriging suffer from severe computational burdens when handling high-dimensional problems or large samples. Conversely, machine learning algorithms such as extreme learning machines exhibit high computational efficiency but lack variance output and stability, making them difficult to employ for adaptive active learning strategies. To address these limitations, this study proposes a population Monte Carlo method based on an adaptive closed neuron extreme learning machine. First, a closed neuron strategy uses a consistency metric to screen and retain neurons containing the most informative features. This preserves the fast analytical solution advantage of extreme learning machines while significantly improving the reconstruction accuracy and stability of the true limit state surface. Second, to overcome the lack of variance in the output, an ensemble model is constructed. By calculating predictive mean and standard deviation, a learning function is formulated for efficient adaptive sample enrichment. Finally, utilizing the adaptive importance sampling mechanism of the population Monte Carlo framework, the auxiliary density function is optimized to progressively shift the sampling center toward high contribution failure regions. Four engineering examples confirm that the proposed method achieves exceptional computational efficiency and high accuracy for complex reliability analysis involving extremely small failure probabilities.

KEYWORDS: Structural reliability analysis; machine learning models; enhanced learning framework; population Monte Carlo; feature screening

1 Introduction

Engineering systems are inevitably affected by uncertainties arising from material properties, geometric dimensions, external loads, and boundary conditions. These uncertainties have a direct influence on structural performance and safety. Structural reliability analysis provides a probabilistic framework to quantify the likelihood of failure under uncertain conditions [1–3]. The main objective of this framework is to estimate the failure probability P_f and the corresponding reliability index β, which are widely used indicators for assessing the safety level of engineering systems [4–7]. A variety of probabilistic approaches have been developed for structural reliability analysis. These approaches are commonly classified into analytical methods and simulation-based methods [8]. Analytical techniques, including first-order and second-order reliability methods, moment-based methods, and saddle point approximations, offer high computational efficiency for problems with moderate nonlinearity and dimensionality [9–12]. Keshtegar et al. [13] combined support

vector regression and the first-order reliability method enhanced by nonlinear conjugate mapping. This approach overcomes the limitations of traditional analytical methods in calculating the failure probability of complex systems. However, their accuracy may deteriorate when the Limit State Function (LSF) exhibits strong nonlinearity, discontinuity, or implicit dependence on random variables [14,15]. To ensure robustness, advanced formulations often require complex iterative procedures and additional convergence criteria, which limit their applicability to large-scale engineering problems [16–18].

Simulation-based methods provide a more general solution for reliability analysis. Monte Carlo Simulation (MCS) is widely regarded as a reference approach due to its simplicity and accuracy [19,20]. It can handle arbitrary probability distributions and complex LSFs without restrictive assumptions. Nevertheless, accurate estimation of small failure probabilities requires a very large number of samples [21]. Therefore, Jafari-Asl et al. [22] developed an improved reliability analysis method based on linear sampling and combined with metaheuristic algorithms, which is very effective for problems involving highly nonlinear or dimensionally complex implicit limit state functions. However, when each sample involves finite element analysis or other expensive numerical models, the computational burden becomes prohibitive. This limitation restricts the direct application of MCS in practical reliability analysis of complex structures [23]. To address this challenge, hybrid reliability frameworks that combine simulation methods with surrogate models have been extensively investigated [24]. In these frameworks, a surrogate model is constructed to approximate the LSF, and MCS is performed on the surrogate instead of the original model [25]. The efficiency of this strategy depends strongly on the accuracy of the surrogate, particularly in the vicinity of the failure boundary [26]. Even small approximation errors in this region may lead to significant deviations in the estimated failure probability and reliability index [27].

Polynomial response surface methods and Kriging models are among the most commonly used surrogate techniques in reliability analysis [28–30]. These methods perform well for low-dimensional problems with smooth response surfaces. Their performance degrades as the number of random variables increases or when strong nonlinearity is present. In such cases, a large number of training samples is required to calibrate the surrogate, which reduces computational efficiency [31]. Similar limitations have been reported for other statistical surrogate models in high-dimensional reliability problems [32]. In recent years, machine learning-based surrogate models have attracted increasing attention due to their strong nonlinear approximation capability [33]. Artificial Neural Networks (ANN), support vector machines, and tree-based models have been successfully applied to structural reliability analysis [34–36]. These models are particularly suitable for problems involving implicit or black box LSFs. However, their training procedures often rely on iterative optimization algorithms, which increase computational cost and require careful parameter tuning [37–39]. ANNs are among the most widely used machine learning surrogates in this field. When sufficient training data are available, they can provide accurate predictions for highly nonlinear LSFs. Nevertheless, the number of unknown parameters grows rapidly with network complexity, leading to increased computational burden in high-dimensional problems. Radial basis neural networks offer a simpler structure, but their performance is sensitive to the selection of centers and shape parameters, especially in high-dimensional spaces [40].

In recent years, modern deep learning surrogates, such as Gaussian Processes (GPs) and Bayesian Neural Networks (BNNs), have been increasingly utilized due to their inherent ability to provide rigorous uncertainty quantification, which is essential for active learning. However, these methods suffer from severe computational bottlenecks. GPs require the inversion of covariance matrices, leading to a computational complexity of $O(N^3)$ that scales poorly with large sample sizes [4,6]. On the other hand, BNNs estimate weight distributions rather than deterministic point estimates, typically relying on Markov Chain Monte Carlo or variational inference. This process introduces massive computational overhead and requires complex hyperparameter tuning, hindering their direct application in structural reliability problems requiring

rapid dynamic updating. Therefore, finding a balance between extreme computational efficiency and reliable predictive variance remains a challenge.

Extreme Learning Machine (ELM) provides an alternative neural framework with significantly reduced training cost [41]. In this approach, the weights and biases between input and hidden layers are randomly generated, and the output weights are determined analytically through least squares regression. This training strategy avoids iterative optimization and enables fast model construction. As a result, ELM is attractive for surrogate-assisted reliability analysis, particularly when the number of training samples is limited. Despite its computational efficiency, the prediction accuracy of ELM is not always satisfactory for reliability analysis. The random generation of hidden layer parameters may produce hidden nodes that contribute little to the approximation of the failure surface. Increasing the number of hidden nodes can partially improve accuracy, but it may also introduce numerical instability and poor generalization performance. These issues limit the direct use of ELM as a surrogate model in structural reliability analysis. From a reliability perspective, only a subset of hidden nodes is truly informative for capturing the failure boundary. Hidden nodes with weak correlation to the structural response may introduce noise and reduce surrogate accuracy. This observation suggests that a systematic screening mechanism is required to identify and retain informative hidden nodes while discarding ineffective ones, without sacrificing the computational efficiency of ELM.

To address the above-mentioned problems, this study combines an adaptive closed-neuron ELM with the population Monte Carlo method and proposes a novel structural reliability analysis method. The main contributions of this method are as follows:

1. First, a closed-neuron strategy based on correlation screening is proposed, which fundamentally optimizes the underlying architecture of the ELM. By innovatively introducing a consistency metric, a systematic feature screening mechanism is established. This mechanism can accurately identify and retain the most informative hidden-layer neurons while removing ineffective nodes. Thus, the model reconstruction accuracy and generalization stability are improved while fully preserving the fast analytical solution advantage of the ELM.
2. Second, a new active learning mechanism is constructed based on ensemble learning, which solves the problem of variance prediction for fast surrogate models. Since a single ELM cannot directly output prediction variance, this study develops an ensemble model of closed-neuron ELMs. Cognitive uncertainty is quantified by calculating the predicted mean and standard deviation of multiple models. On this basis, a corresponding learning function is formulated. It drives the surrogate model to adaptively enrich samples in key high-uncertainty regions near the failure boundary. This avoids the heavy computational difficulty faced by traditional Gaussian processes in inverting covariance matrices.
3. This study deeply couples adaptive active learning with the population Monte Carlo sampling framework. During the construction of the surrogate model, the sampling center gradually and accurately shifts toward failure regions with high contribution. This effectively overcomes the limitation of excessive computational cost caused by matrix operations of traditional surrogate models with large-scale samples. It also avoids the waste of computing resources caused by blind sampling and accelerates the convergence of extremely small failure probabilities under complex nonlinear limit states.

Finally, strict verification using multiple complex engineering cases shows that the proposed method can accurately capture high-dimensional and complex failure boundaries. With a limited number of real model evaluations, the method achieves a magnitude improvement in computational efficiency for structural reliability analysis.

The remainder of this paper is organized as follows. Section 2 introduces the theoretical background of reliability analysis, with emphasis on MCS and several representative traditional machine learning

models. Section 3 presents the main theoretical framework of this study, providing a detailed description of the adaptive construction process of the adaptive closed ELM model and its integration with reliability analysis based on the Population Monte Carlo (PMC) method. Section 4 presents four engineering examples and compares the advantages and limitations of the proposed reliability analysis approach with several traditional reliability analysis methods. Section 5 summarizes the main contributions of this study and outlines the primary directions for future research.

2 Theoretical Basis of Reliability Analysis

2.1 The Theoretical Basis of Monte Carlo

The fundamental principle of Monte Carlo-based structural reliability analysis is to evaluate the structural limit state function using a massive number of random samples generated from the joint probability distributions of basic variables, thereby estimating the probability of failure as the mathematical expectation of the failure domain indicator function according to the Law of Large Numbers [42]. Numerical simulation experiments are then conducted, and according to the law of large numbers the frequency of event occurrence approaches the corresponding probability, which enables the estimation of structural reliability. The structural performance function is expressed as $y = g(\boldsymbol{x})$. The vector $\boldsymbol{x} = (x_1, x_2, \ldots, x_n)^T$ denotes the basic random variables, and its probability density function is $f_x(\boldsymbol{x})$. Random sampling of the basic variables $\boldsymbol{x}$ is performed N times according to $f_x(\boldsymbol{x})$. Each sample is substituted into the LSF to obtain $g\left(\boldsymbol{x}^j\right)$, where $j = 1, 2, \ldots, N$. The number of samples satisfying $g\left(\boldsymbol{x}^j\right) < 0$ is denoted as n_f. The failure probability can therefore be estimated as follows:

$$P_f = \int_F f_x(\boldsymbol{x})dx = \int_{\mathbb{R}^n} I_F\left(g(\boldsymbol{x})\right) f_x(\boldsymbol{x})dx = E\left(I_F\left(g\left(\boldsymbol{x}\right)\right)\right) \tag{1}$$

where, P_f is the failure probability, F denotes the failure domain defined by $\{x: g\left(x\right) < 0\}$, $\mathbb{R}^n$ represents the n-dimensional real space, $I_F\left(g(\boldsymbol{x})\right)$ is the failure domain indicator function which equals 1, if $g\left(\boldsymbol{x}\right) < 0$ and 0 otherwise, and $E\left(\cdot\right)$ denotes the mathematical expectation operator.

The mathematical expectation of the failure domain indicator function can be approximated by the sample mean. Specifically, the ratio between the number of samples that fall within the failure domain defined by $\{\boldsymbol{x}: g\left(\boldsymbol{x}\right) < 0\}$ and the total number of samples N is calculated. The estimated structural failure probability is therefore expressed as follows:

$$\hat{P}_f = \frac{1}{N}\sum_{i=1}^{N} I_F\left(g(\boldsymbol{x})\right) = \frac{n_f}{N} \tag{2}$$

where $\hat{P}_f$ represents the estimated structural failure probability. The coefficient of variation of the estimated structural failure probability $Cov\left(\hat{P}_f\right)$ can be expressed as follows:

$$Cov\left(\hat{P}_f\right) = \frac{\sqrt{Var\left(\hat{P}_f\right)}}{E\left(\hat{P}_f\right)} \approx \sqrt{\frac{1-\hat{P}_f}{(N-1)\,\hat{P}_f}} \tag{3}$$

where, $Var\left(\hat{P}_f\right)$ denotes the sample variance, which can be estimated as $Var\left(\hat{P}_f\right) = \left(\hat{P}_f - \hat{P}_f^2\right) / (N-1)\,\hat{P}_f$.

The number of randomly generated sample points in the MCS directly affects the accuracy of the estimated structural reliability. Therefore, when the MCS is used to analyze events with small failure probabilities, a very large number of samples must be generated in order to obtain results that satisfy the required accuracy, which leads to low computational efficiency. To overcome the limitations of low efficiency

and large computational cost associated with the MCS, improved sampling strategies can be employed to evaluate structural reliability, including Importance Sampling (IS), directional sampling, and stratified sampling techniques.

2.2 MCS Based on Surrogate Models

However, with the continuous increase in the complexity of engineering systems, the LSF of a structure often exhibits implicit characteristics [43]. This implies that there is no explicit analytical mathematical expression that directly describes the relationship between the input random variables and the structural response through algebraic operations. Each evaluation of the structural state must therefore rely on highly time-consuming numerical analysis procedures to obtain an implicit solution.

At the same time, in order to satisfy the high safety requirements of modern engineering systems, the probability of structural failure is usually extremely small, typically on the order of 10^{-4} or even lower than 10^{-6} [44]. To accurately capture these extremely rare failure events while ensuring that the coefficient of variation of the estimated failure probability remains within an acceptable range, it is often necessary to generate millions of samples. This requirement can lead to an exponentially increasing computational cost, making the direct application of the MCS in practical engineering problems face severe computational and time-related limitations.

To address the problem of excessive computational cost when applying the MCS to complex structural reliability analysis involving implicit LSFs, surrogate modeling techniques replace the implicit LSF with an approximated explicit function. Through iterative sampling and model updating, the convergence of the estimated failure probability can be ensured. Common surrogate models include the response surface method, the Kriging method, and multilayer perceptron models. Among these approaches, multilayer perceptron models possess several notable advantages compared with other surrogate models. According to the universal approximation theorem, when a sufficient number of hidden neurons is available, multilayer perceptron models are capable of approximating any continuous nonlinear function with arbitrary accuracy. In addition, for high dimensional problems, such methods are able to automatically perform feature extraction and dimensionality reduction. Common multilayer perceptron models include the following.

2.2.1 Artificial Neural Network

In ANN, the predicted output is expressed as:

$$\hat{H}_{ANN}(\mathbf{X}) = \sum_{j=1}^{M} w_j \Theta\left(\sum_{i=1}^{n} w_{ji} X_i + b_j\right) + b \tag{4}$$

where $\hat{H}_{ANN}(\mathbf{X})$ is the predicted output of the ANN for the input vector X, M represents the total number of hidden neurons, n is the dimension of the input variables, X_i is the i-th input variable, w_j denotes the weight connecting the j-th hidden neuron to the output node, and w_{ji} represents the weight connecting the i-th input variable to the j-th hidden neuron. The parameters b_j and b are bias terms. The function $\Theta(\cdot)$ is a nonlinear activation function. In this study, the sigmoid function is adopted.

The total number of unknown coefficients increases rapidly with the number of input variables and hidden neurons. These coefficients are commonly determined through back-propagation-based optimization. In this work, the Levenberg-Marquardt algorithm is employed to minimize the mean squared error between predicted and observed responses. Although ANN provides strong nonlinear approximation capability, the iterative training process increases computational cost [45], especially for high-dimensional problems.

2.2.2 Radial Basis Neural Network

Radial basis neural network also consists of three layers, but its hidden layer employs radial basis functions for nonlinear mapping [46]. The hidden neuron response is defined as:

$$\hat{H}_{RBNN}(\mathbf{X}) = \exp\left(-\frac{\| \mathbf{X} - \mathbf{c}_j \|^2}{2\sigma^2}\right) \tag{5}$$

where $\hat{H}_{RBNN}(\mathbf{X})$ denotes the output response of the radial basis neural network, $\mathbf{c}_j$ denotes the center of the j-th hidden neuron, σ is the shape parameter controlling the spread of the basis function, and $\|\cdot\|$ represents the Euclidean norm. Compared with ANN, the number of unknown coefficients in the radial basis neural network is reduced. The model performance is sensitive to the selection of centers and shape parameters. In this study, a radial basis neural network is trained using backpropagation with the Levenberg-Marquardt algorithm. Although the training process is simpler than that of an ANN, parameter selection remains a critical issue.

2.2.3 Extreme Learning Machine

ELM uses a single hidden-layer feedforward network as originally proposed by Huang et al. [47], but its training strategy differs from back-propagation-based models. For an input vector $X \in \mathbb{R}^n$, the surrogate prediction is written as:

$$\hat{H}_{ELM}(X) = \sum_{j=1}^{M} \beta_j \Theta\left(\sum_{i=1}^{n} a_{ji} X_i + b_j\right) \tag{6}$$

where $\hat{H}_{ELM}(X)$ is the predicted output of the ELM, n is the dimension of the input vector X, M is the number of hidden neurons and $\Theta(\cdot)$ is the activation function. The parameters a_{ji} and b_j denote the weights and biases connecting the input layer to the hidden layer. In ELM, these parameters are randomly generated and remain fixed during training. The coefficients β_j connect the hidden layer to the output layer and are solved analytically.

Assume that N training samples $\left\{X^{(k)}, Y^{(k)}\right\}_{k=1}^{N}$ are available, where $Y^{(k)}$ is the observed value of the LSF at $X^{(k)}$. The network output on the training set can be written in matrix form as:

$$H\beta \approx Y \tag{7}$$

where $Y = \left[Y^{(1)}, \ldots, Y^{(N)}\right]^{\top} \in \mathbb{R}^N$, $\beta = [\beta_1, \ldots, \beta_M]^{\top} \in \mathbb{R}^M$, and $H \in \mathbb{R}^{N \times M}$ is the hidden layer output matrix. Each entry of H is computed by:

$$H_{kj} = \Theta\left(\sum_{i=1}^{n} a_{ji} X_i^{(k)} + b_j\right) \tag{8}$$

which represents the response of the j-th hidden neuron to the k-th training input. The output weights are obtained by solving a least squares problem that minimizes the training residual $\| H\beta - Y \|_2$. A standard solution is:

$$\beta = H^{\dagger} Y \tag{9}$$

where $H^{\dagger}$ denotes the Moore–Penrose pseudoinverse of H. This closed-form training avoids iterative optimization and provides high computational efficiency when compared with back-propagation-based networks [47]. However, the randomness in input weights can lead to fluctuating generalization performance.

3 The Proposed Method

When addressing small failure probability problems, the computational cost required by MCS is extremely high. IS can effectively reduce the computational cost of reliability analysis by concentrating samples in regions where failure is more likely to occur. To address complex engineering problems, this study proposes the use of an improved ELM to replace the true LSF. A typical IS strategy, namely the population MCS, is adopted to construct the auxiliary probability density function. IS points are generated according to the auxiliary probability density function and are treated as candidate samples. From these candidate samples, the most informative training points are selected to update the ELM model. After each training iteration, the surrogate limit state surface changes, which requires the approximate optimal auxiliary probability density function to be recalculated and new importance samples to be generated. This iterative process continues until the stopping criterion is satisfied. The proposed method is referred to as the adaptive closed ELM population Monte Carlo method (ACELM-PMC).

3.1 Importance Sampling

As illustrated in Fig. 1, unlike MCS, in which the sampling center is located at the coordinate origin, IS employs a probability density function that is easy to sample, denoted as $h(\boldsymbol{u})$, and satisfies the condition that the expectation of $I_F(\boldsymbol{u})/h(\boldsymbol{u})$ under $h(\boldsymbol{u})$ exists. The indicator function $I_F(\boldsymbol{u})$ can therefore be rewritten as $\frac{I_F(\boldsymbol{u})}{h(\boldsymbol{u})}h(\boldsymbol{u})$, and sampling is performed with respect to $h(\boldsymbol{u})$. In this way, the sampling center is shifted from the coordinate origin to regions that make significant contributions to the estimation of the failure probability. The failure probability can therefore be expressed as follows:

$$P_f = \int_{R^n} I_F(\boldsymbol{u}) f(\boldsymbol{u}) d\boldsymbol{u} = \int_{R^n} I_F(\boldsymbol{u}) \frac{f(\boldsymbol{u})}{h(\boldsymbol{u})} h(\boldsymbol{u}) d\boldsymbol{u} \tag{10}$$

where $\boldsymbol{u}$ represents the random variable vector transformed into the standard normal space, $h(\boldsymbol{u})$ denotes the auxiliary density function, $f(\boldsymbol{u})$ denotes the probability density function, and R^n represents the n dimensional variable space.

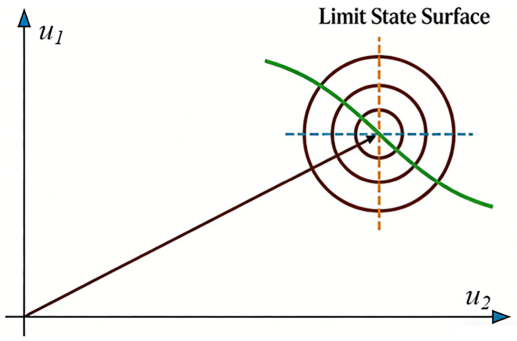

Figure 1: Principle of importance sampling.

By selecting more representative samples corresponding to failure states and assigning appropriate weights to these samples, they are given greater importance in reliability computation, which helps reduce the estimation variance of the failure probability. When simulation samples $\left\{\boldsymbol{u}^{(i)}, i = 1, \ldots, n_{IS}\right\}$ are generated using the auxiliary density function $h(\boldsymbol{u})$, the failure probability can be calculated as follows:

$$\hat{P}_f = E\left[I_F(\boldsymbol{u}) \frac{f(\boldsymbol{u})}{h(\boldsymbol{u})}\right] = \frac{1}{n_{IS}} \sum_{i=1}^{n_{IS}} I_F\left(\boldsymbol{u}^{(i)}\right) \frac{f\left(\boldsymbol{u}^{(i)}\right)}{h\left(\boldsymbol{u}^{(i)}\right)} \tag{11}$$

The coefficient of variation can be calculated as follows:

$$Cov\left(\hat{P}_f\right) = \frac{\sqrt{Var\left(\hat{P}_f\right)}}{\hat{P}_f} \tag{12}$$

where, $Var\left(\hat{P}_f\right)$ represents the variance of $\hat{P}_f$, and the corresponding expression is given as follows:

$$Var\left(\hat{P}_f\right) = \frac{1}{n_{IS}}\left[\frac{1}{n_{IS}}\sum_{i=1}^{n_{IS}} I_F\left(\boldsymbol{u}^{(i)}\right)\frac{f^2\left(\boldsymbol{u}^{(i)}\right)}{h\left(\boldsymbol{u}^{(i)}\right)} - \hat{P}_f^2\right] \tag{13}$$

Sampling from $h(\boldsymbol{u})$ enables efficient exploration of important regions. The construction of $h(\boldsymbol{u})$ is the core component of the IS method. The properties of $h(\boldsymbol{u})$ determine whether IS can improve sampling efficiency and whether the estimated failure probability remains unbiased. In this study, the population MCS is employed to construct $h(\boldsymbol{u})$.

3.2 Population Monte Carlo Method

The PMC method is a technique for complex probabilistic analysis and can be regarded as an improvement and extension of IS [48]. It approximates the probability distribution of a complex system by maintaining a set of solutions. Each solution represents a potential realization of the system. Through iterative updates of the solution set, the particles in the set gradually evolve toward samples drawn from the target distribution. Statistical analysis of the resulting sample set is then performed to obtain various properties of the target distribution. The PMC belongs to the class of adaptive IS methods. Its main procedure is summarized as follows:

Step 1: A set of randomly generated particles is initialized as the initial solution set of the population. The size of this solution set is usually determined according to the scale of the problem.

Step 2: For each particle, a weight is assigned according to the distance between the represented solution and the target distribution. In general, particles that are closer to the target distribution are assigned larger weights, whereas particles that are farther away are assigned smaller weights.

Step 3: After the particle weights are evaluated, importance resampling is performed according to the particle weights to update the population. High-quality particles have a greater probability of being retained, whereas low-quality particles are typically eliminated.

Step 4: The procedure is iterated by repeating Steps 2 and 3 until the particle distribution in the population becomes stable.

Finally, the failure probability is estimated through statistical analysis of the sample set. In order to obtain IS points, the selection of the proposal distribution and the resampling procedure must be performed.

3.2.1 Selection of the Proposal Distribution

Cappe and coauthors proposed the use of a single distribution with different distribution parameters as the proposal distribution [49]. However, such a proposal distribution has limited exploration capability in the state space. To address this limitation, a proposal distribution composed of a mixture of multiple distributions has been developed. The mathematical expression of the proposal distribution is described as follows:

$$\psi^{(t)}(\boldsymbol{u}) = \frac{1}{N_{po}}\sum_{k=1}^{N_{po}} q_k^{(t)}\left(u\left|\Lambda_k^{(t)}, \Sigma_k^{(t)}\right.\right) \tag{14}$$

where $\psi^{(t)}(\boldsymbol{u})$ is the mixture proposal distribution at iteration t, $q_k^{(t)}$ denotes the k-th component distribution, $q_k^{(t)}\left(u\left|\Lambda_k^{(t)},\Sigma_k^{(t)}\right.\right)$ denotes the $q_k^{(t)}$ component distribution, t denotes the iteration index, N_{po} represents the number of proposal distributions, $\Lambda_k^{(t)}$ denotes the location parameter, and $\Sigma_k^{(t)}$ denotes the scale parameter. As illustrated in Fig. 2, k_{po} samples are generated from each distribution $q_k^{(t)}\left(u\left|\Lambda_k^{(t)},\Sigma_k^{(t)}\right.\right)$, respectively.

$$u_{i,k}^{(t)} \sim q_k^{(t)}\left(\boldsymbol{u}\left|\Lambda_k^{(t)},\Sigma_k^{(t)}\right.\right), i=1,\ldots,k_{po} \tag{15}$$

where $u_{i,k}^{(t)}$ represents the i-th sample generated from the k-th component distribution $q_k^{(t)}$ at iteration t.

The particles generated by all proposal distributions can be expressed as $\left\{u_{1,1}^{(t)},\ldots,u_{i,k_{po}}^{(t)},\ldots,u_{N_{po},1}^{(t)},\ldots,u_{N_{po},k_{po}}^{(t)}\right\}$. The total number of samples is $N_{pmc}=N_{po}\times k_{po}$. The resampling weight coefficient of particle $u_{i,k}^{(t)}$ is given as follows:

$$\varpi_{i,j}^{(t)}=\frac{\tilde{p}_c\left(u_{i,k}^{(t)}\right)}{\psi^{(t)}\left(u_{i,k}^{(t)}\right)} \tag{16}$$

where, $\tilde{p}_c(\boldsymbol{u})$ denotes the approximate optimal auxiliary density function, which can be expressed as follows:

$$\tilde{p}_c(\boldsymbol{u})=\pi_c(\boldsymbol{u})\,\phi(\boldsymbol{u}) \tag{17}$$

where, $\phi(\boldsymbol{u})$ denotes the probability density function of the standard normal distribution and $\pi_c(\boldsymbol{u})$ denotes the probability classification function, which can be calculated as follows:

$$\pi_c(\boldsymbol{u})=P\{\hat{g}(\boldsymbol{u})<0\}=\phi\left(-\frac{\hat{\mu}_g(\boldsymbol{u})}{\hat{\sigma}_g(\boldsymbol{u})}\right) \tag{18}$$

where, $\hat{g}(\boldsymbol{u})$ denotes the predicted value of the surrogate model, while $\hat{\mu}_g(\boldsymbol{u})$ and $\hat{\sigma}_g(\boldsymbol{u})$ represent the predictive mean and the predictive standard deviation of the surrogate model at point $\boldsymbol{u}$, respectively.

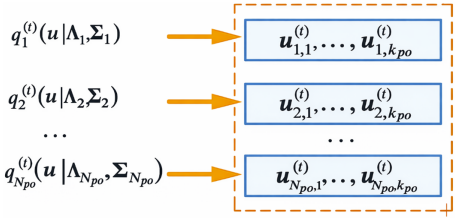

Figure 2: Multi-distribution proposal distribution.

3.2.2 Resampling Technique

As shown in Eq. (14), when the true probability density value $\tilde{p}_c\left(\boldsymbol{u}_i^{(t)}\right)$ of particle $\boldsymbol{u}_i^{(t)}$ is large and the approximate probability density $\psi^{(t)}\left(u_{i,k}^{(t)}\right)$ is small, the weight $\boldsymbol{u}_i^{(t)}$ becomes large. This indicates that when a particle makes a significant contribution to the failure probability calculation in Eq. (11) and the difference between the approximate probability density and the true probability density is large, that particle tends to be assigned a larger weight. During the resampling process, the resampled particles gradually move toward the locations of particles that have larger weights in the previous iteration. After a sufficient

number of iterations, the proposal distribution gradually approaches the target distribution, and the particles progressively concentrate in regions that contribute significantly to the failure probability calculation.

Before resampling, the particle weights must be normalized. Particularly in high-dimensional spaces, the standard PMC multi-distribution proposal process inherently suffers from the curse of dimensionality. As the number of dimensions increases, the variance of the importance weights tends to explode, making it exponentially difficult for a finite mixture of proposal distributions to adequately cover the failure domain. This phenomenon leads to severe particle degeneracy. When global normalization is adopted, some proposal distribution components may be far from the target distribution, resulting in extremely small particle weights. During resampling, these components may be eliminated, which leads to a reduction in diversity. To alleviate this dimension-induced particle degeneracy during resampling and to enhance the exploration capability of the state space, local normalization of the particle weights has been proposed [50] and adopted in this study. While local normalization significantly improves robustness in problems of moderate dimensionality, the capacity of the multi-distribution proposal to efficiently explore ultra-high-dimensional spaces remains a fundamental limitation. The detailed definition of the normalized weights is given as follows:

$$\overline{\omega}_{i,j}^{(t)} = \frac{\omega_{i,j}^{(t)}}{\sum_{j=1}^{k_{po}} \omega_{i,j}^{(t)}}, i = 1, \ldots, N_{po} \tag{19}$$

where $\overline{\omega}_{i,j}^{(t)}$ denotes the normalized resampling weight coefficient for the corresponding particle. The PMC method adopts multinomial resampling to perform the resampling procedure. The particles obtained through resampling are used to iteratively update the distribution parameters of the proposal distribution. After the iterative process terminates, the IS simulation samples $\left\{\boldsymbol{u}^{(i)}, i = 1, \ldots, n_{IS}\right\}$ are obtained.

3.3 Adaptive Construction Procedure of the ACELM Model

3.3.1 Architecture of the ACELM Model

ELM constructs a single hidden-layer network with randomly generated input weights and biases, and then computes the output weights by least squares. This training strategy is fast. Its prediction accuracy, however, depends strongly on the hidden neurons. When the number of hidden neurons M is small, the nonlinear mapping capacity is limited. When M is large, the regression step may become less stable. In reliability analysis, another issue becomes critical. Many randomly generated hidden neurons have weak relevance to the limit state response. These neurons contribute little to the approximation of the failure boundary and can reduce accuracy.

To improve accuracy while keeping the same training efficiency, a closed neuron strategy is introduced. A large pool of candidate hidden neurons is generated first. The size of this pool is set to AM, where A is a scale factor and $A \geq 10$ is used in practice. Random weights and biases are sampled in a prescribed interval and used to compute the candidate hidden neuron outputs on the training set. The key step is to screen these candidates and retain only informative neurons before solving the output weights. This converts an unstructured random hidden layer into a compact set of effective hidden neurons.

The screening relies on an agreement measure between each candidate hidden neuron and the observed limit state values on the training samples. Consider N training inputs $X^{(i)}$ and the corresponding observed responses $Y^{(i)}$. Let $h_j^{(i)}$ denote the output of the j-th candidate hidden neuron evaluated at $X^{(i)}$. The agreement index ρ_j of the j-th neuron is defined by:

$$\rho_j = \frac{\sum_{i=1}^{N}\left(h_j^{(i)} - \overline{h}_j\right)\left(Y^{(i)} - \overline{Y}\right)}{\sqrt{\sum_{i=1}^{N}\left(h_j^{(i)} - \overline{h}_j\right)^2}\sqrt{\sum_{i=1}^{N}\left(Y^{(i)} - \overline{Y}\right)^2}} \tag{20}$$

where $\overline{h}_j$ and $\overline{Y}$ represent their corresponding sample means over the N training samples. Eq. (20) mathematically represents the Pearson correlation coefficient between the individual hidden neuron output and the target limit state values. The fundamental background for utilizing this specific index lies in the mathematical architecture of the ELM. In ELM, while the mapping from the input space to the hidden layer is nonlinear, the final predictive output is strictly a linear combination of these hidden-layer feature maps. Therefore, assessing the linear dependency between a hidden neuron's activation h_j and the target response Y aligns perfectly with the underlying linear regression mechanism of the ELM output layer.

The specific rationale for selecting this index as the screening criterion is twofold. First, hidden nodes with a low absolute value of ρ_j provide negligible informative variance for the final linear combination and essentially act as numerical noise. Filtering them out prevents ill-conditioned matrix inversion issues during the least squares calculation, thereby significantly enhancing the generalization stability of the model. Second, the calculation of this correlation index is computationally highly efficient, which strictly preserves the ultra-fast analytical training advantage of the ELM framework without introducing the heavy computational burden typical of iterative feature selection algorithms.

Two selection rules are employed. In the fixed size rule, all candidates are ranked by $|\rho_j|$ and the top M neurons are kept. All remaining neurons are closed. This rule produces a fixed model size and stable computation. In the self-active rule, the number of retained neurons is determined by a statistical threshold. Let μ_ρ and σ_ρ be the mean and standard deviation of ρ_j across all candidates. A neuron is retained if it satisfies:

$$\rho_j \geq \mu_\rho + k\sigma_\rho \tag{21}$$

where $k \in [-1, 1]$ controls the strictness of screening. A larger k produces fewer active neurons. A smaller k retains more neurons and increases model flexibility. The scale factor A influences the diversity of candidates. A larger A increases the chance of generating neurons with strong agreement. These two parameters control the balance between accuracy and efficiency.

After screening, the hidden layer output matrix is constructed using only the retained neurons. The output weights are then obtained by the same least squares solution as standard ELM. The closed neuron mechanism changes only the hidden layer composition and does not alter the regression form. In Fig. 3, the candidate neurons are generated first, then the ineffective ones are removed, and finally, the reduced network framework is trained. This sequence clarifies that the screening is a preprocessing step that improves the quality of the hidden representation.

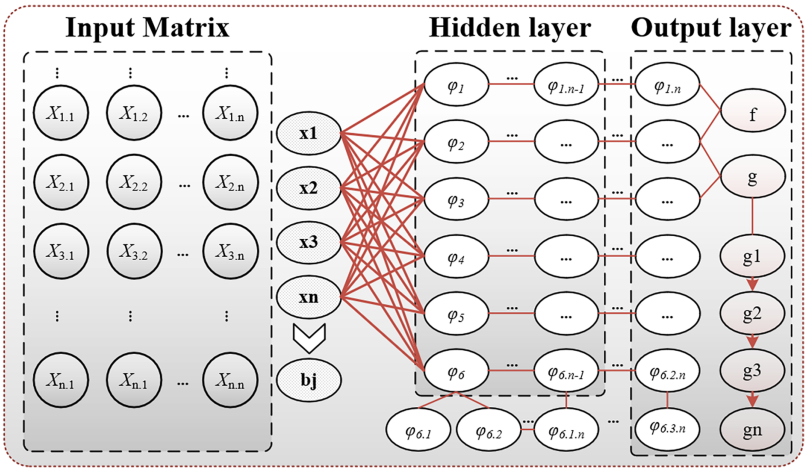

Figure 3: Schematic of the proposed closed-neuron ELM.

3.3.2 Adaptive Modeling

To address the insufficient specificity of the aforementioned ACELM for the failure boundary defined by $g(\boldsymbol{u}) = 0$ during its construction, this study presents an adaptive construction strategy for ACELM. The detailed implementation procedure is outlined as follows:

Step 1: An initial ACELM model is trained using Design of Experiments (DOE) with a sample size of N.

Step 2: Predictions are conducted for candidate sample points, and the prediction variance of ACELM at each point is calculated.

Step 3: The sample point that is most likely to lie on the failure boundary and exhibits the highest uncertainty is selected and incorporated into the DOE.

Step 4: The true response of the selected point is obtained via mathematical simulation, and the ACELM model is retrained.

Step 5: The preceding steps are repeated iteratively until the model fully converges near the failure boundary.

To enhance the construction efficiency of ACELM, the training sample set should be updated by selecting the most critical samples. Since ACELM only provides predicted values without prediction variance, ensemble learning is adopted in this study to quantify the epistemic uncertainty of the model. The initial stage of ACELM construction involves the random generation of a large number of candidate neurons, leading to minor discrepancies among the final ACELM models even when trained on the same dataset. Accordingly, an ensemble of surrogate models consisting of K-th ACELM models is first established, where K is set to 5 in this study. While a larger ensemble size could statistically yield a smoother and more robust estimation of the predictive variance, its improvement on the actual sampling efficiency of the U-learning function exhibits diminishing returns. This is because the U-function primarily relies on the relative ranking of uncertainties among candidate points rather than their absolute variance values. Therefore, a small ensemble size like $K = 5$ is empirically sufficient to effectively identify the most informative regions. Furthermore, notably, the non-iterative and extremely fast analytical reconstruction characteristic of ACELM enables automatic updating of these five models within milliseconds. Unlike GPs that compute variance through expensive covariance matrix operations, or BNNs that require heavy probabilistic training, the non-iterative and extremely fast analytical reconstruction characteristic of ACELM enables automatic updating of these

ensemble models within milliseconds. This ensemble strategy provides a highly efficient approximation of the epistemic uncertainty without sacrificing computational speed.

For the candidate sample pool $\boldsymbol{X}^{(i)}$, the set $\{\hat{g}_1(\boldsymbol{X}), \ldots, \hat{g}_K(\boldsymbol{X})\}$ of prediction outputs from each ACELM model is computed individually. The predicted mean $\mu_{\hat{g}(\boldsymbol{X})}$ and predicted standard deviation $\sigma_{\hat{g}(\boldsymbol{X})}$ for each sample point are subsequently derived accordingly:

$$\mu_{\hat{g}(\boldsymbol{X})} = \frac{1}{K}\sum_{i=1}^{K}\hat{g}_i(\boldsymbol{X}) \tag{22}$$

$$\sigma_{\hat{g}(\boldsymbol{X})} = \sqrt{\frac{1}{K-1}\sum_{i=1}^{K}\left(\hat{g}_i(\boldsymbol{X}) - \mu_{\hat{g}(\boldsymbol{X})}\right)^2} \tag{23}$$

A larger predicted standard deviation $\sigma_{\hat{g}(\boldsymbol{X})}$ indicates lower prediction confidence of the model at the corresponding point. Inspired by the U function, a learning function for ACELM is defined as:

$$U(\boldsymbol{X}) = \frac{\left|\mu_{\hat{g}(\boldsymbol{X})}\right|}{\sigma_{\hat{g}(\boldsymbol{X})}} \tag{24}$$

where $U(\boldsymbol{X})$ is the learning function value evaluating the informative value of candidate point $\boldsymbol{X}$. The updated point to be selected is given as follows:

$$\boldsymbol{x}^* = arg\min_{\boldsymbol{x}\in\boldsymbol{X}} U(\boldsymbol{X}) \tag{25}$$

where $\boldsymbol{x}^*$ denotes the optimal updated point to be selected, and $\boldsymbol{X}$ represents the candidate sample pool. In addition, the stopping criterion for the ensemble ACELM is described as follows:

$$\min U(\boldsymbol{X}) \geq 2 \tag{26}$$

In this case, the confidence level that the predicted value is positive or negative reaches 97.7%, and the updating process can therefore be terminated. Although the predictive distribution of the ensemble ACELM does not strictly follow a Gaussian distribution, it is approximately assumed in engineering practice that the prediction error follows a Gaussian distribution so that the U function can be employed as the stopping criterion.

3.4 The Group Monte Carlo Method Based on Adaptive ACELM

As shown in Fig. 4, the procedural flow of the ACELM-PMC method is presented, and the detailed steps are described as follows:

Step 1: Transform the random variable $\boldsymbol{x}$ into the standard normal variable $\boldsymbol{u}$;

Step 2: Several samples are extracted using the Latin Hypercube Sampling (LHS) method as the initial DOE. 20 samples are extracted in this study;

Step 3: An initial ensemble of ACELM models is constructed based on the initial DOE;

Step 4: The normal distributions denoted by $\left\{N\left(u\left|\Lambda_k^{(t)}, \Sigma_k^{(t)}\right.\right), k = 1, \ldots, N_{po}\right\}$ are used as the proposal distributions of the PMC method with the iteration number $t = 1$. $\Lambda_k^{(t)}$) and $\Sigma_k^{(t)}$ represent the mean and standard deviation of the k-th normal distribution, respectively. The initial parameters $\Lambda_k^{(t)}$ are generated randomly and $\Sigma_k^{(t)}$ is defined as the identity matrix. A sufficiently large value of N_{po} is recommended to ensure the exploration ability of the PMC method in the state space;

Step 5: Generate k_{po} samples from each distribution $N\left(u\left|\Lambda_k^{(t)},\Sigma_k^{(t)}\right.\right)$, denoted as $\left\{u_{1,1}^{(t)},\ldots,u_{i,k_{po}}^{(t)},\ldots,u_{N_{po},1}^{(t)},\ldots,u_{N_{po},k_{po}}^{(t)}\right\}$;

Step 6: Calculate the weight $\left\{\varpi_{i,j}^{(t)},i=1,\ldots,N_{po},j=1,\ldots,k_{po}\right\}$ for each sample;

Step 7: Normalize the weights $\left\{\varpi_{i,j}^{(t)},i=1,\ldots,N_{po},j=1,\ldots,k_{po}\right\}$ to $\left\{\overline{\varpi}_{i,j}^{(t)},i=1,\ldots,N_{po},j=1,\ldots,k_{po}\right\}$;

Step 8: Perform polynomial resampling based on the weights and particles $\left(u_{i,j}^{(t)},\varpi_{i,j}^{(t)}\right)$ to obtain particles $\left\{\boldsymbol{ur}_{i,j}^{(t)},i=1,\ldots,N_{po},j=1,\ldots,k_{po}\right\}$, and update the mean of the proposal distribution as follows:

$$\Lambda_k^{(t+1)}=\frac{1}{k_{po}}\sum_{j=1}^{k_{po}}\boldsymbol{ur}_{i,j}^{(t)},k=1,\ldots,N_{po} \tag{27}$$

where $\boldsymbol{ur}_{i,j}^{(t)}$ represents the particles obtained after the multinomial resampling process, and $\Sigma_k^{(t+1)}$ represents the identity matrix;

Step 9: Generate k_{po} samples from each distribution $N\left(u\left|\Lambda_k^{(t+1)},\Sigma_k^{(t+1)}\right.\right)$, denoted as $\left\{u_{1,1}^{(t+1)},\ldots,u_{i,k_{po}}^{(t+1)},\ldots,u_{N_{po},1}^{(t+1)},\ldots,u_{N_{po},k_{po}}^{(t+1)}\right\}$;

Step 10: Calculate the response value of each sample and determine the number n_p of samples located in the failure domain. When n_p is greater than $\rho\times N_{po}\times k_{po}$, the particles $\left\{\boldsymbol{u}_{1,1}^{(t+1)},\ldots,u_{i,k_{po}}^{(t+1)},\ldots,u_{N_{po},1}^{(t+1)},\ldots,u_{N_{po},k_{po}}^{(t+1)}\right\}$ are recorded as important sample points denoted as $\left\{\boldsymbol{u}^{(i)},i=1,\ldots,n_{IS}\right\}$ and proceed to Step 11. Otherwise, return to Step 10: The parameter ρ is used to judge the convergence of the PMC method and $\rho=0.5$ in this study. The calculation procedure of n_p is described as follows:

$$n_p=\sum_{i=1}^{N_{po}}\sum_{j=1}^{k_{po}}I_F\left(\mu_g\left(\boldsymbol{u}_{i,j}^{(t)}\right)\right) \tag{28}$$

where n_p is the number of samples located in the failure domain, and $\mu_g\left(\boldsymbol{u}_{i,j}^{(t)}\right)$ denotes the predictive mean of the surrogate model ensemble for sample $\boldsymbol{u}_{i,j}^{(t)}$;

Step 11: Judge whether the accuracy of the current ensemble ACELM model meets the required criteria. If the accuracy satisfies the requirement, proceed to Step 14. Otherwise, proceed to Step 12;

Step 12: Select the optimal training point from the set $\left\{\boldsymbol{u}^{(i)},i=1,\ldots,n_{IS}\right\}$ using the U function and add it to the DOE;

Step 13: Update the ensemble ACELM model according to the revised DOE with the newly added training point and return to Step 4;

Step 14: Calculate the structural failure probability and the coefficient of variation of the failure probability using the simulation samples $\left\{\boldsymbol{u}^{(i)},i=1,\ldots,n_{IS}\right\}$.

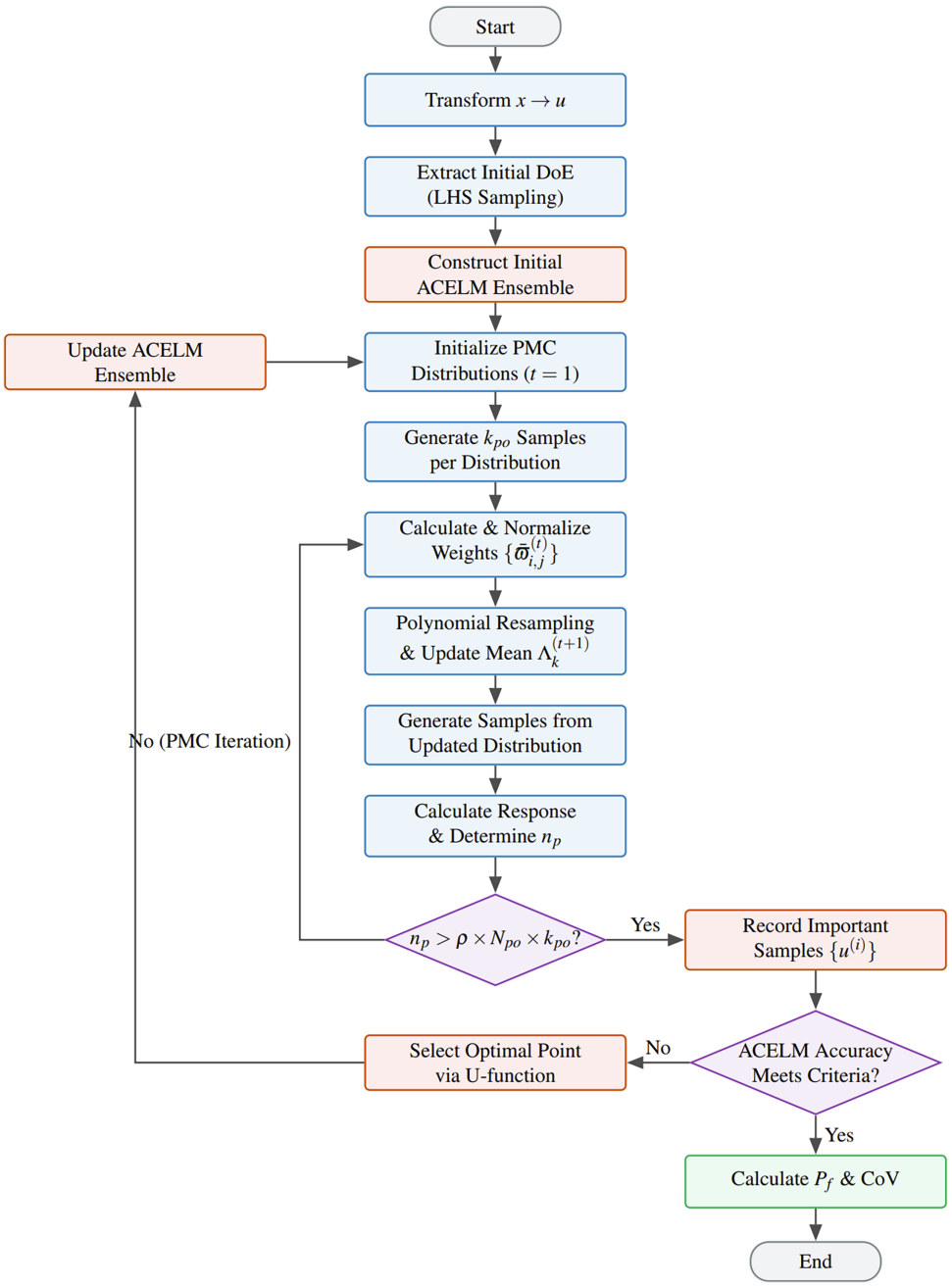

Figure 4: Method flow of ACELM-PMC.

4 Numerical Validation

In this section, the generalization ability, approximation accuracy, and computational efficiency of the proposed reliability analysis method ACELM-PMC are rigorously evaluated. In this section, comparisons are made among the reference results based on MCS, the computational results of MCS assisted by the active Kriging model (AK-MCS), those of IS assisted by the active Kriging model (AK-IS), and those of MCS based on ELM (ELM-MCS), so as to examine the surrogate model construction efficiency, as well as the computational efficiency and accuracy of reliability indices for the proposed method. Among them,

the parameters of ACELM-PMC are N_{po} = 50 and k_{po} = 200; in the updating process of Kriging, the U-function is adopted to select new training samples, and the number of initial sample points is 12 unless otherwise specified; the candidate pool expansion factor used in the ACELM model is A = 100, and the adaptive selection threshold is k = −0.5.

The rationale for this parameter selection is based on the trade-off between the richness of the feature pool and network stability. Since generating random hidden nodes in ELM incurs almost no computational cost, choosing a large-scale factor of A = 100 guarantees a sufficiently rich candidate pool from which highly informative features can be extracted. Regarding the adaptive selection threshold k, setting k = −0.5 slightly relaxes the screening strictness compared to the mean level where k = 0. This preserves a moderate degree of neuron diversity to prevent underfitting while effectively eliminating irrelevant noise neurons.

Extensive empirical tests indicate that the final calculated reliability index is highly insensitive to parameter A when A takes a sufficiently large value of 10 or greater. For the threshold k, reliability estimation remains highly stable across a broad and appropriate interval from −0.7 to −0.2. However, extreme values of k will degrade model performance. Assigning k a value that is too high, such as any value greater than 0.5, causes over-screening and underfitting due to an insufficient number of neurons. In contrast, assigning k a value that is too low, such as −1, retains an excessive number of uninformative nodes and leads to numerical instability as well as a higher coefficient of variation.

In addition, in the computational results, N_{call} denotes the number of calls to the limit-state function, Pf_{pre} denotes the calculated failure probabilities by different methods, Cov_{pre} denotes the coefficient of variation of the different computational results, T means the actual execution time consumed in one experiment and err denotes the relative error of the different computational results with respect to the reference solution based on MCS. Furthermore, to test the robustness of the proposed method, 30 replicate experiments with only different random samples are conducted. The computer used in this study is Intel (R) Core (TM) i9-9900K CPU @ 3.60 GHz, using a 64-bit operating system.

4.1 Nonlinear Mathematical Examples

In this example, a highly nonlinear two-dimensional function is adopted, whose objective function is defined as [51]:

$$G(X) = sin\left(\frac{5x_1}{2}\right) - \frac{\left(x_1^2 + 4\right)(x_2 - 1)}{20} + 3 \tag{29}$$

where, $x_1 \sim N(1.5, 1)$, $x_1 \sim N(2.5, 1)$. Table 1 presents the calculation results of different reliability methods.

Table 1: Reliability analysis results of nonlinear mathematical example.

Methods	Sample Size	N_{call}	Pf_{pre}	Cov_{pre}	T (s)	err
MCS	10^7	–	2.59×10^{-3}	0.062%	1.5	–
AK-MCS	10^6	34.4	2.57×10^{-3}	0.55%	23.1	0.77%
AK-IS	10^6	31.7	2.38×10^{-3}	2.26%	30.4	8.10%
ELM-MCS	10^6	50	2.53×10^{-3}	4.16%	25.6	2.32%
ACELM-PMC	10^6	25.9	2.58×10^{-3}	1.43%	22.9	0.39%

It can be seen from the table that the calculation result of MCS is 2.59×10^{-3} with extremely high stability. By comparing different surrogate model-based reliability methods, it can be found that AK-IS has the lowest calculation accuracy. This may be because when IS is used to solve highly nonlinear

problems, if the constructed IS density function cannot fully cover the complex failure domain or the global optimal design point cannot be found, serious curse of dimensionality or local bias will occur, leading to prediction distortion. In addition, ELM-MCS does not adopt an adaptive construction strategy. To obtain a sufficiently accurate model, the size of the training dataset is manually set to 50. A comparison of the actual computational times consumed by different reliability analysis methods reveals that ACELM-PMC and Kriging-MCS are the two most computationally efficient approaches. Among them, ACELM-PMC incurs a lower computational cost while achieving higher computational accuracy.

Fig. 5 shows the surrogate limit state surface and the sampled importance points after convergence of ACELM-PMC. It can be seen from Fig. 5 that almost all the generated importance sample points are located in the failure region that contributes significantly to the failure, rather than in the circular region centered at the origin. This greatly reduces the number of analysis sample points.

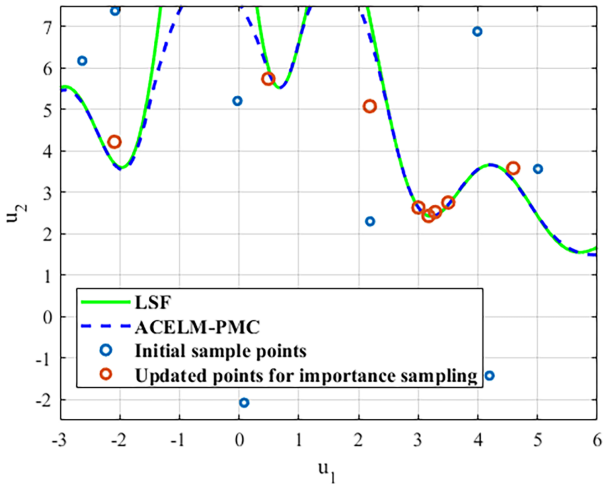

Figure 5: Converged surrogate limit state surface and training points.

In addition, Fig. 6 shows the boxplot of the number of LSF evaluations called by different reliability analysis methods during 30 repeated experiments. It can be seen that ACELM-PMC exhibits better robustness in the repeated experiments.

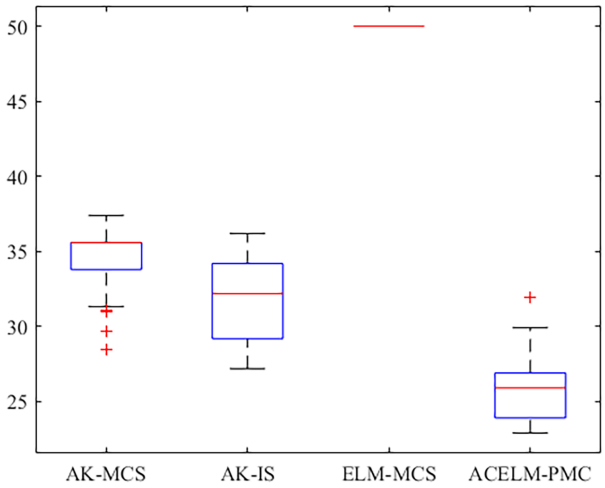

Figure 6: Number of LSF calls for different surrogate models.

4.2 Failure Problem of a Hollow Cantilever Beam Structure

Fig. 7 shows a hollow cantilever beam structure. The cantilever beam is subjected to external forces F_1 (kN), F_2 (kN), P (kN) and torque T (N/m). The angle between F_1 and the z-direction is $\theta_1 = 5^\circ$, and the angle between F_2 and the z-direction is $\theta_2 = 10^\circ$. The structure fails when the maximum stress of the cantilever beam exceeds the yield strength S_y (MPa) of the material. The performance function is defined as [41]:

$$g\left(t, d, L_1, L_2, F_1, F_2, P, T, S_y\right) = S_y - \sqrt{\sigma_x^2 + 3\tau_{zx}^2} \tag{30}$$

where σ_x denotes the normal stress, τ_{zx} denotes the shear stress. σ_x and τ_{zx} can be calculated as:

$$\begin{cases} \sigma_x = \dfrac{P + F_1 sin\left(\theta_1\right) + F_2 sin\left(\theta_1\right)}{\dfrac{\pi}{4}\left[d^2 - (d-2t)^2\right]} + \dfrac{d\left(F_1 L_1 cos\left(\theta_1\right) + F_2 L_2 cos\left(\theta_2\right)\right)}{\dfrac{\pi}{2}\left[d^4 - (d-2t)^4\right]} \\ \tau_{zx} = \dfrac{Td}{d^4 - (d-2t)^4} \end{cases} \tag{31}$$

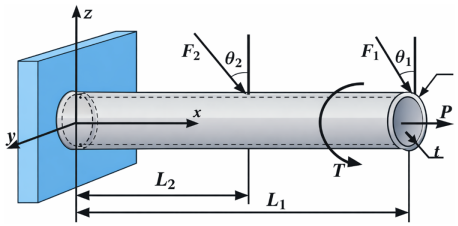

Figure 7: Hollow cantilever beam.

In this example, the input variables are mutually independent, and their statistical information is listed in Table 2.

Table 2: Input variable information for the hollow cantilever beam structure.

Variables	Distribution Types	Parameters
t (m)	Normal distribution	N (5, 0.1)
d (mm)	Normal distribution	N (42, 0.5)
L_1 (mm)	Uniform distribution	U (119.75, 120.25)
L_2 (mm)	Uniform distribution	U (59.75, 60.25)
F_1 (kN)	Normal distribution	N (3, 0.3)
F_2 (kN)	Normal distribution	N (3, 0.3)
P (kN)	Gumbel distribution	Mean = 12, Standard deviation = 1.2
T (N/m)	Normal distribution	N (90, 9)
S_y (MPa)	Normal distribution	N (220, 22)

Table 3 presents the calculation results of ACELM-PMC and other reliability analysis methods.

Table 3: Reliability analysis results of failure problem of a hollow cantilever beam structure.

Methods	Sample Size	N_{call}	Pf_{pre}	Cov_{pre}	T (s)	err
MCS	10^8	–	1.529×10^{-4}	0.81%	30.7	–
AK-MCS	10^6	151	1.506×10^{-4}	2.72%	73.9	1.50%
AK-IS	10^6	99	1.505×10^{-4}	5.27%	157.7	1.57%
ELM-MCS	10^6	200	1.502×10^{-4}	2.57%	90.9	1.77%
ACELM-PMC	10^6	31	1.510×10^{-4}	1.73%	59.4	1.24%

It can be seen from the table that the coefficient of variation of the MCS calculation results is very low, indicating extremely high stability. By comparing the other four surrogate model-based reliability analysis methods, it is clear that all surrogate model methods have successfully reduced the sample size required for calculating the failure probability to one million. This demonstrates the significant advantage of surrogate models in replacing time-consuming finite element analysis. In terms of the number of LSF evaluations and actual execution time, ACELM-PMC only requires 31 evaluations to achieve high-precision modeling, and its computation time is much lower than that of ordinary ELM or active Kriging models. Regarding the accuracy of the calculation results, AK-MCS effectively reduces the difficulty and cost of reliability analysis. Although AK-IS reduces the number of LSF evaluations, it has a very high coefficient of variation, indicating insufficient robustness. This may be due to the inherent geometric matching deviation between the proposed sampling distribution and the actual failure domain distribution. Even with fewer evaluations, large estimation variance is inevitably introduced, leading to a significantly higher coefficient of variation. In addition, the ordinary ELM lacks a built-in predictive uncertainty evaluation mechanism. It cannot accurately locate the most informative sample points during iteration and can only passively rely on numerous random samples to describe the global boundary. Therefore, it requires the largest number of evaluations and is prone to local fitting errors. As a result, the error of the ordinary ELM-assisted MCS reaches 1.77%, and its surrogate model accuracy is the poorest. In contrast, ACELM not only provides the neural network with adaptive optimization feature extraction ability to accurately capture the key regions that contribute most to the failure probability, but also efficiently screens from a large candidate pool through advanced pattern recognition algorithms. It can be seen that ACELM performs the best among different reliability analysis methods.

4.3 Planar Truss Failure Problem

This example considers a planar truss consisting of 23 members, as shown in Fig. 8 [52]. The truss contains 11 horizontal members and 12 diagonal members. The cross-sectional areas and elastic moduli of the horizontal and diagonal members are denoted as $A_1\left(\mathrm{cm}^2\right)$, $A_2\left(\mathrm{cm}^2\right)$, E_1 (GPa), and E_2 (GPa), respectively. The truss is subjected to six concentrated forces P_1 (kN) ~ P_6 (kN) on the top horizontal members. All ten variables are treated as random variables, and their distribution parameters are listed in Table 4. The structure fails when the deflection at Node 1 exceeds 14 cm. Therefore, the LSF of this example is expressed as:

$$g\left(A_1, A_2, E_1, E_2, P_1, \ldots, P_6\right) = 0.14 - \left|\delta_{max}\left(x\right)\right| \tag{32}$$

where $\delta_{max}\left(x\right)$ stands for the deflection of Node 1, calculated by finite element programs.

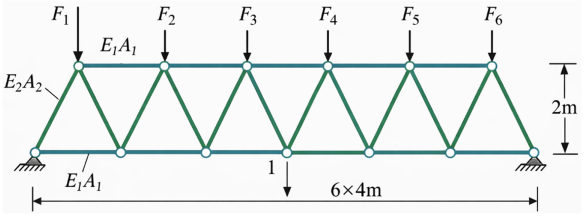

Figure 8: Dimensional parameters of the planar truss.

Table 4: Input variable information in the planar truss failure problem.

Variables	Distribution Types	Means	Standard Deviations
E_1 (GPa)	Log-normal distribution	210	21
E_2 (GPa)	Log-normal distribution	210	21
A_1 (cm^2)	Log-normal distribution	20	2
A_2 (cm^2)	Log-normal distribution	10	1
P_1 (kN)	Gumbel distribution	50	7.5
P_2 (kN)	Gumbel distribution	50	7.5
P_3 (kN)	Gumbel distribution	50	7.5
P_4 (kN)	Gumbel distribution	50	7.5
P_5 (kN)	Gumbel distribution	50	7.5
P_6 (kN)	Gumbel distribution	50	7.5

The calculation results of different reliability methods for this example are listed in Table 5.

Table 5: Reliability analysis results of the planar truss failure problem.

Methods	Sample Size	N_{call}	Pf_{pre}	Cov_{pre}	T (s)	err
MCS	10^7	–	3.44×10^{-5}	0.76%	27.4	–
AK-MCS	10^7	462	3.30×10^{-5}	3.68%	41.6	4.06%
AK-IS	10^7	356	3.32×10^{-5}	5.46%	53.2	3.48%
ELM-MCS	10^7	400	3.49×10^{-5}	6.78%	68.7	1.45%
ACELM-PMC	10^7	159	3.47×10^{-5}	1.83%	34.5	0.87%

The failure probability of this example is very low. As shown in the calculation results in the table, the performance of traditional reliability analysis methods, including AK-MCS, AK-IS, and ELM-MCS, decreases slightly for low failure probability problems compared with other problems. In contrast, ACELM-MCS exhibits the best performance in terms of coefficient of variation and relative error among all methods, demonstrating its applicability to low failure probability problems. For low failure probability problems, traditional modeling methods must rely on massive computing resources to blindly search for update points of the surrogate model or sample points located in the failure region. Although the active learning Kriging model can use the prediction variance inherent in the Gaussian process to guide samples to accumulate near the limit state surface, its correlation function cannot perfectly map the real physical topology when dealing with the complex failure boundary of the planar truss. This often leads to more iterative calls and remaining high errors. On the one hand, ACELM-PMC solves the difficulty of collecting efficient update points. On the other hand, it improves the efficiency and accuracy of failure probability calculation.

4.4 Failure Problem of Anti-Roll Torsion Bar under Ultimate Load

As shown in Fig. 9, this example considers an anti-roll torsion bar, which mainly bears torsional load during the vehicle body roll. It is mainly composed of a connecting rod, a torsion arm, and a torsion bar shaft. The torsion bar shaft and the torsion arm are connected by an interference fit. The torsion bar shaft is a cylindrical structure with variable cross-sections. Circular transitions are adopted at the transition parts of the torsion arm mounting seat and the support seat of the torsion bar shaft. The 1/2 structure and dimensions of the torsion bar shaft are shown in Fig. 10. As shown in Fig. 11, two forces F_1 (kN) with equal magnitude and opposite directions act on the torsion arms through the connecting rods from the vehicle body. The torsion bar shaft maintains balance with the external force through the supporting force of the mounting seat and the torque generated by itself.

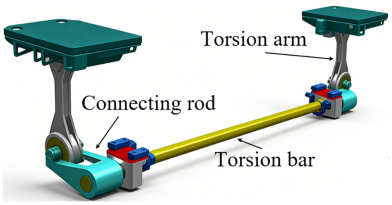

Figure 9: Anti-roll torsion bar device.

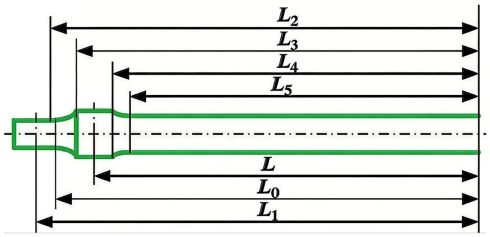

Figure 10: Half structure and dimensions of the torsion bar shaft.

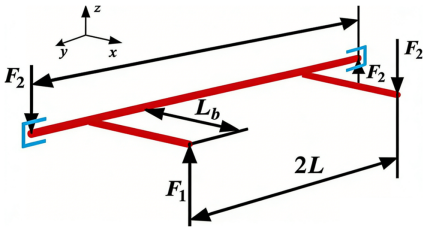

Figure 11: Force analysis of the torsion bar shaft and torsion arm in the anti-roll torsion bar device.

It can be seen from Fig. 10 that the torsion bar shaft has a variable cross-section structure. In this study, the engineering method for calculating the stress of variable cross-section shafts proposed in Reference [53] is used to calculate the stress of the torsion bar shaft. According to the geometric shape and stress state of the torsion bar shaft, the maximum stress appears at the following positions:

(1) the cross-section with the combined maximum bending moment and torque;
(2) the surface with stress concentration;
(3) the position with the minimum diameter;
(4) the initial cross-section of the interference fit.

Based on the above principles, six calculation cross-section positions, namely A~F, are determined, as shown in Fig. 12. Among them, cross-sections A, C and D are the initial surfaces of the interference fit; cross-sections B and E are the regions with stress concentration; cross-section F is a pure torsion cross-section.

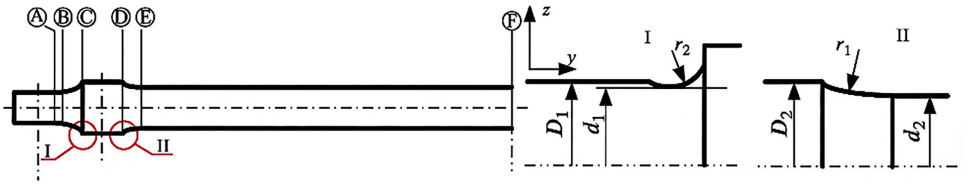

Figure 12: Calculated cross-section positions of the torsion bar shaft.

This section considers an anti-roll torsion bar for a high-speed train, manufactured from 52CrMoV4 steel. During train operation, it bears the ultimate working load F_1. The torsion bar shaft fails when the maximum stress $\sigma_{\max}$ exceeds the yield strength of the material or the maximum shear stress $\tau_{\max}$ exceeds the shear yield strength. The performance function can be defined as:

$$G = \min \begin{cases} \sigma_s - \sigma_{\max} \\ \tau_s - \tau_{\max} \end{cases} \tag{33}$$

where, σ_s = 1300 MPa represents the yield strength of the manufacturing material, and τ_s = 750 MPa represents the shear yield strength of the manufacturing material. The parameters of the input variables are listed in Table 6, where d_F (m) is the diameter of the circular cross-section F.

Table 6: Input variable information in the failure problem of anti-roll torsion bar under ultimate load.

Variables	Distribution Types	Parameters
L_1 (m)	Normal distribution	N (1292, 10)
$F_{1,\max}$ (kN)	Normal distribution	N (60, 6)
d_F (m)	Normal distribution	N (53, 2)
E (GPa)	Normal distribution	N (210, 2.1)
G (GPa)	Normal distribution	N (80, 0.8)

The calculation results of different reliability methods are described in Table 7.

Table 7: Reliability analysis results of the anti-roll torsion bar failure problem.

Methods	Sample Size	N_{call}	Pf_{pre}	Cov_{pre}	T (s)	err
MCS	10^6	–	2.62×10^{-3}	0.76%	48.9	–
AK-MCS	10^6	64	2.65×10^{-3}	1.91%	98.7	1.14%
AK-IS	10^6	36	2.50×10^{-3}	2.02%	169.3	4.58%
ELM-MCS	10^6	400	2.72×10^{-3}	1.98%	118.9	2.81%
ACELM-PMC	10^6	18	2.58×10^{-3}	1.68%	72.0	1.52%

It can be seen from the calculation data in the table that ACELM-PMC shows relatively good accuracy and computational efficiency. Although AK-MCS has the best calculation accuracy, ACELM only requires 18 LSF evaluations while maintaining similar accuracy, which greatly improves computational efficiency. Compared with traditional AK-IS and ELM-MCS, ACELM-PMC achieves significant improvements in both accuracy and stability. This demonstrates that the ACELM model effectively enhances the performance of ELM and verifies the effectiveness and superiority of combining ACELM with PMC for reliability analysis.

5 Conclusion

In structural reliability analysis, surrogate models based on active learning have been widely adopted. Nevertheless, existing surrogate models confront substantial challenges: they suffer from model inadaptation when addressing high-dimensional problems or large datasets; some high-performance models are difficult to directly employ for constructing adaptive active learning strategies, and their generalization performance tends to fluctuate considerably. To this end, this study proposes a PMC based on an adaptive closed ELM.

By introducing a neuron closure strategy, the approach intelligently selects and retains the most informative neurons for the target response from a large random candidate pool. While preserving the ultra-fast analytical solution advantage of the ELM, it improves the reconstruction accuracy and stability of the actual limit-state surface. Inspired by the ensemble learning paradigm, an adaptive closed ELM is constructed to achieve efficient adaptive sample enrichment assisted by the U-function. This high-efficiency surrogate model is deeply integrated with the adaptive IS mechanism within the PMC framework, which continuously optimizes the auxiliary probability density function and drives the sampling center to shift accurately and persistently toward the high-contribution failure regions.

Finally, the effectiveness and superiority of the proposed method are verified through four complex engineering examples. The primary research findings are summarized as follows:

1. The proposed ACELM-PMC achieves a magnitude improvement in computational efficiency for extremely small failure probability problems. It requires significantly fewer limit state function evaluations compared to traditional Kriging and standard ELM-assisted Monte Carlo methods while maintaining stringent accuracy.
2. The closed-neuron screening strategy effectively identifies and removes uninformative hidden nodes. This innovation fundamentally resolves the numerical instability and poor generalization issues of traditional ELM, without sacrificing its ultra-fast analytical training advantage.
3. The customized ensemble learning paradigm successfully equips the ELM framework with predictive uncertainty quantification capabilities. This enables robust and active exploration of high-uncertainty regions near complex failure boundaries, entirely overcoming the drawback of blind sampling in ordinary ELM surrogates.

However, when constructing the active learning function and defining the iterative stopping criterion, the present method approximately assumes that the prediction error of the ensemble ACELM follows a Gaussian distribution, which is not strictly valid and may compromise the accuracy of sample updating under certain highly nonlinear extreme conditions. Furthermore, while the proposed closed-neuron screening strategy inherently performs a degree of dimensionality reduction by filtering out uninformative features, scaling the active learning framework to ultra-high-dimensional problems remains a formidable challenge. In such extremely high-dimensional spaces, the exponential growth of the sample volume severely dilutes the initial DOEs, making it difficult for any surrogate model to locate the failure region efficiently. Future research will focus on integrating deep dimensionality reduction techniques with ACELM, exploring generalized

uncertainty quantification indicators without strict distributional assumptions, and developing intelligent adaptive optimization mechanisms to further conquer ultra-high-dimensional reliability problems.

Acknowledgement: Not applicable.

Funding Statement: The authors received no specific funding for this study.

Author Contributions: The authors confirm contribution to the paper as follows: Conceptualization, Yunlong Teng, Ying Liu, Jianhong Liang and Jinshang Luo; methodology, Yunlong Teng, Ying Liu, Jianhong Liang and Jinshang Luo; software, Yunlong Teng, Ying Liu, Jianhong Liang and Jinshang Luo; validation, Yunlong Teng, Ying Liu, Jianhong Liang and Jinshang Luo; formal analysis, Jianhong Liang and Jinshang Luo; investigation, Yunlong Teng and Ying Liu; resources, Yunlong Teng, Ying Liu, Jianhong Liang and Jinshang Luo; data curation, Yunlong Teng; writing—original draft preparation, Yunlong Teng and Ying Liu; writing—review and editing, Yunlong Teng, Ying Liu and Jianhong Liang; visualization, Jinshang Luo; supervision, Jinshang Luo; project administration, Yunlong Teng, Ying Liu, Jianhong Liang and Jinshang Luo; funding acquisition, Yunlong Teng, Ying Liu, Jianhong Liang and Jinshang Luo. All authors reviewed and approved the final version of the manuscript.

Availability of Data and Materials: The data that support the findings of this study are available from the Corresponding Author, [Jinshang Luo], upon reasonable request.

Ethics Approval: Not applicable.

Conflicts of Interest: The authors declare no conflicts of interest.

Abbreviations

LSF	Limit State Function
MCS	Monte Carlo simulation
ANN	Artificial Neural Networks
GP	Gaussian Processe
BNN	Bayesian Neural Network
ELM	Extreme Learning Machine
IS	Importance Sampling
PMC	Population Monte Carlo
ACELM-PMC	Adaptive closed ELM population Monte Carlo method
DOE	Design of Experiments
AK-MCS	The computational results of MCS assisted by the active Kriging model
AK-IS	IS assisted by the active Kriging model
ELM-MCS	MCS based on ELM

References

1. Zhang H, Song LK. Active learning surrogates in system reliability analysis: a review. Int J Struct Integr. 2025;10(21):1–52. doi:10.1108/ijsi-08-2025-0195.
2. Chen X, Li J. A novel approach for structural system reliability evaluation using decoupled first-order reliability method and equivalent extreme-value event. Reliab Eng Syst Saf. 2025;257(2):110851. doi:10.1016/j.ress.2025.110851.
3. Yang S, Meng D, Alfouneh M, Keshtegar B, Zhu SP. A robust-weighted hybrid nonlinear regression for reliability based topology optimization with multi-source uncertainties. Comput Methods Appl Mech Eng. 2025;447(2):118360. doi:10.1016/j.cma.2025.118360.
4. Dang C, Beer M. Semi-Bayesian active learning quadrature for estimating extremely low failure probabilities. Reliab Eng Syst Saf. 2024;246(2):110052. doi:10.1016/j.ress.2024.110052.

5. Li C, Wen JR, Wan J, Taylan O, Fei CW. Adaptive directed support vector machine method for the reliability evaluation of aeroengine structure. Reliab Eng Syst Saf. 2024;246(4):110064. doi:10.1016/j.ress.2024.110064.
6. Zhang Y, Dong Y, Xu J. An accelerated active learning Kriging model with the distance-based subdomain and a new stopping criterion for reliability analysis. Reliab Eng Syst Saf. 2023;231(1):109034. doi:10.1016/j.ress.2022.109034.
7. Meng Z, Zhang Z, Li G, Zhang D. An active weight learning method for efficient reliability assessment with small failure probability. Struct Multidiscip Optim. 2020;61(3):1157–70. doi:10.1007/s00158-019-02419-z.
8. Saraygord Afshari S, Enayatollahi F, Xu X, Liang X. Machine learning-based methods in structural reliability analysis: a review. Reliab Eng Syst Saf. 2022;219:108223. doi:10.1016/j.ress.2021.108223.
9. Zhao YG, Ono T. A general procedure for first/second-order reliabilitymethod (FORM/SORM). Struct Saf. 1999;21(2):95–112. doi:10.1016/S0167-4730(99)00008-9.
10. Meng D, Yang H, Yang S, Zhang Y, De Jesus AMP, Correia J, et al. Kriging-assisted hybrid reliability design and optimization of offshore wind turbine support structure based on a portfolio allocation strategy. Ocean Eng. 2024;295(5):116842. doi:10.1016/j.oceaneng.2024.116842.
11. Huang P, Li H, Gu Y, Qiu G. An extended moment-based trajectory accuracy reliability analysis method of robot manipulators with random and interval uncertainties. Reliab Eng Syst Saf. 2024;246(4):110082. doi:10.1016/j.ress.2024.110082.
12. Hu Z, Mansour R, Olsson M, Du X. Second-order reliability methods: a review and comparative study. Struct Multidiscip Optim. 2021;64(6):3233–63. doi:10.1007/s00158-021-03013-y.
13. Keshtegar B, El Amine Ben Seghier M, Zio E, Correia JAFO, Zhu SP, Trung NT. Novel efficient method for structural reliability analysis using hybrid nonlinear conjugate map-based support vector regression. Comput Methods Appl Mech Eng. 2021;381(3):113818. doi:10.1016/j.cma.2021.113818.
14. Xie B, Wang Y, Zhu Y, Liu P, Wu Y, Lu F. Time-variant reliability analysis of angular contact ball bearing considering the coupled effect of rolling contact fatigue damage and wear. Reliab Eng Syst Saf. 2024;241:109667. doi:10.1016/j.ress.2023.109667.
15. Zhang B, Wang W, Wang Y, Li Y, Li CQ. A critical review on methods for time-dependent structural reliability. Sustain Resilient Infrastruct. 2024;9(2):91–106. doi:10.1080/23789689.2023.2206297.
16. Zhu SP, Keshtegar B. Brief introduction on reliability methods. In: Structural reliability analysis: analytical methods. Cham, Switzerland: Springer Nature; 2025. p. 27–84. doi:10.1007/978-3-031-75197-4_2.
17. Meng D, Li Y, He C, Guo J, Lv Z, Wu P. Multidisciplinary design for structural integrity using a collaborative optimization method based on adaptive surrogate modelling. Mater Des. 2021;206(2):109789. doi:10.1016/j.matdes.2021.109789.
18. Chen X, Li J. A decoupled first-order reliability method for the time-dependent structural system reliability evaluation from the perspective of probability density evolution. Reliab Eng Syst Saf. 2025;266(2):111629. doi:10.1016/j.ress.2025.111629.
19. Papadrakakis M, Papadopoulos V, Lagaros ND. Structural reliability analyis of elastic-plastic structures using neural networks and Monte Carlo simulation. Comput Methods Appl Mech Eng. 1996;136(1–2):145–63. doi:10.1016/0045-7825(96)01011-0.
20. Gordini M, Habibi MR, Tavana MH, TahamouliRoudsari M, Amiri M. Reliability analysis of space structures using Monte-Carlo simulation method. Structures. 2018;14(ST6):209–19. doi:10.1016/j.istruc.2018.03.011.
21. Sun H, Bao Y. An active learning method based on Monte Carlo dropout neural network for high-dimensional reliability analysis. Reliab Eng Syst Saf. 2025;262(2):111169. doi:10.1016/j.ress.2025.111169.
22. Jafari-Asl J, Ohadi S, El Amine Ben Seghier M, Trung NT. Accurate structural reliability analysis using an improved line-sampling-method-based slime mold algorithm. ASCE-ASME J Risk Uncertainty Eng Syst Part A Civ Eng. 2021;7(2):04021015. doi:10.1061/ajrua6.0001129.
23. Hong L, Li S, Chen M, Xu P, Li H, Cheng J. Non-probabilistic reliability analysis with both multi-super-ellipsoidal input and fuzzy state. Comput Methods Appl Mech Eng. 2024;429:117154. doi:10.1016/j.cma.2024.117154.
24. Zhou C, Zhang H, Chang Q, Song X, Li C. An adaptive ensemble of surrogate models based on hybrid measure for reliability analysis. Struct Multidiscip Optim. 2021;65(1):16. doi:10.1007/s00158-021-03129-1.

25. Li Y, Luo Y, Zhong Z. An active sparse polynomial chaos expansion approach based on sequential relevance vector machine. Comput Methods Appl Mech Eng. 2024;418(4):116554. doi:10.1016/j.cma.2023.116554.
26. Chu H, Li W, Sun D, Liu Z, Zheng W, Xu J, et al. AK-MCS structural reliability analysis method based on improved active learning function. J Reliab Sci Eng. 2025;1(2):025003. doi:10.1088/3050-2454/add161.
27. Ghiasi M, Ghadimi N, Ahmadinia E. An analytical methodology for reliability assessment and failure analysis in distributed power system. SN Appl Sci. 2018;1(1):44. doi:10.1007/s42452-018-0049-0.
28. Alibrandi U. A response surface method for stochastic dynamic analysis. Reliab Eng Syst Saf. 2014;126(3):44–53. doi:10.1016/j.ress.2014.01.003.
29. Yang S, Meng D, Wang H, Yang C. A novel learning function for adaptive surrogate-model-based reliability evaluation. Philos Trans A Math Phys Eng Sci. 2024;382(2264):20220395. doi:10.1098/rsta.2022.0395.
30. Ranjan P, Haynes R, Karsten R. A computationally stable approach to Gaussian process interpolation of deterministic computer simulation data. Technometrics. 2011;53(4):366–78. doi:10.1198/TECH.2011.09141.
31. Gao S, Zhao Y, Zhao X, Zhang Y. Application of response surface method based on new strategy in structural reliability analysis. Structures. 2023;57(2):105202. doi:10.1016/j.istruc.2023.105202.
32. Ji Y, Liu H, Xiao NC, Zhan H. An efficient method for time-dependent reliability problems with high-dimensional outputs based on adaptive dimension reduction strategy and surrogate model. Eng Struct. 2023;276(2):115393. doi:10.1016/j.engstruct.2022.115393.
33. Luo J, Ma X, Ji Y, Li X, Song Z, Lu W. Review of machine learning-based surrogate models of groundwater contaminant modeling. Environ Res. 2023;238(1):117268. doi:10.1016/j.envres.2023.117268.
34. Shafiq A, Çolak AB, Lone SA, Sindhu TN, Muhammad T. Reliability modeling and analysis of mixture of exponential distributions using artificial neural network. Math Methods Appl Sci. 2024;47(5):3308–28. doi:10.1002/mma.8178.
35. Bosio A, Bernardi P, Ruospo A, Sanchez E. A reliability analysis of a deep neural network. In: Proceedings of the 2019 IEEE Latin American Test Symposium (LATS); 2019 Mar 11–13; Santiago, Chile. doi:10.1109/latw.2019.8704548.
36. Zhao Y, Hu K, Fu B, Wang Z, Wang Y, Yao X. Reliability analysis of composite laminate patch repaired structures based on response surface proxy model. Compos Commun. 2023;42:101689. doi:10.1016/j.coco.2023.101689.
37. Bian K, Priyadarshi R. Machine learning optimization techniques: a survey, classification, challenges, and future research issues. Arch Comput Methods Eng. 2024;31(7):4209–33. doi:10.1007/s11831-024-10110-w.
38. Dang C, Valdebenito MA, Faes MGR, Song J, Wei P, Beer M. Structural reliability analysis by line sampling: a Bayesian active learning treatment. Struct Saf. 2023;104(2):102351. doi:10.1016/j.strusafe.2023.102351.
39. Wang J, Li YH, Wang D, Chai M. A reliability calculation method based on ISSA-BP neural network. Int J Struct Integr. 2024;15(6):1249–67. doi:10.1108/IJSI-07-2024-0104.
40. Zhang Y, Ma J, Du W. A new radial basis function active learning method based on distance constraint for structural reliability analysis. Int J Mech Mater Des. 2023;19(3):567–81. doi:10.1007/s10999-023-09644-x.
41. Cheng J, Jin H. An adaptive extreme learning machine based on an active learning method for structural reliability analysis. J Braz Soc Mech Sci Eng. 2021;43(12):546. doi:10.1007/s40430-021-03257-1.
42. Rubinstein RY, Kroese DP. Simulation and the monte Carlo method. Hoboken, NJ, USA: John Wiley & Sons, Inc.; 2016. doi:10.1002/9781118631980.
43. Meng Z, Qian Q, Xu M, Yu B, Yıldız AR, Mirjalili S. PINN-FORM: a new physics-informed neural network for reliability analysis with partial differential equation. Comput Methods Appl Mech Eng. 2023;414:116172. doi:10.1016/j.cma.2023.116172.
44. Eshra E, Papakonstantinou KG, Nikbakht H. A direct importance sampling-based framework for rare event uncertainty quantification in non-Gaussian spaces. Reliab Eng Syst Saf. 2025;264(4):111200. doi:10.1016/j.ress.2025.111200.
45. Kang F, Li JS, Wang Y, Li J. Extreme learning machine-based surrogate model for analyzing system reliability of soil slopes. Eur J Environ Civ Eng. 2017;21(11):1341–62. doi:10.1080/19648189.2016.1169225.
46. Kumar R. Recurrent context layered radial basis function neural network for the identification of nonlinear dynamical systems. Neurocomputing. 2024;580(4):127524. doi:10.1016/j.neucom.2024.127524.

47. Huang GB, Zhu QY, Siew CK. Extreme learning machine: theory and applications. Neurocomputing. 2006;70 (1–3):489–501. doi:10.1016/j.neucom.2005.12.126.
48. Cappé O, Guillin A, Marin JM, Robert CP. Population Monte Carlo. J Comput Graph Stat. 2004;13(4):907–29. doi:10.1198/106186004X12803.
49. Cappé O, Douc R, Guillin A, Marin JM, Robert CP. Adaptive importance sampling in general mixture classes. Stat Comput. 2008;18(4):447–59. doi:10.1007/s11222-008-9059-x.
50. Elvira V, Martino L, Luengo D, Bugallo MF. Generalized multiple importance sampling. Statist Sci. 2019;34(1):129–55. doi:10.1214/18-sts668.
51. Zhou T, Peng Y. An active-learning reliability method based on support vector regression and cross validation. Comput Struct. 2023;276(5):106943. doi:10.1016/j.compstruc.2022.106943.
52. Hong L, Li H, Fu J. A novel surrogate-model based active learning method for structural reliability analysis. Comput Methods Appl Mech Eng. 2022;394:114835. doi:10.1016/j.cma.2022.114835.
53. BS EN 13103-1:2017. Railway applications. In: Wheelsets and bogies—part 1: design method for axles with external journals. London, UK: British Standards Institution; 2017.